Development of supercapacitor systems based on binary and ternary nanocomposites using chitosan, graphene and polyaniline

Anand Torvi , Satishkumar Naik , Mahadevappa Kariduraganavar

PII: S2405-8300(18)30139-3
DOI: https://doi.org/10.1016/j.cdc.2018.11.003
Reference: CDC 161

To appear in: *Chemical Data Collections*

Received date: 5 July 2018
Revised date: 3 November 2018
Accepted date: 5 November 2018

Please cite this article as: Anand Torvi , Satishkumar Naik , Mahadevappa Kariduraganavar , Development of supercapacitor systems based on binary and ternary nanocomposites using chitosan, graphene and polyaniline, *Chemical Data Collections* (2018), doi: https://doi.org/10.1016/j.cdc.2018.11.003

HIGHLIGHTS

- A series of binary (chitosan-polyaniline) and ternary (chitosan-graphene-polyaniline) nanocomposites have been developed via *in-situ* polymerization of aniline.
- The molar ratio of polyaniline and mass ratio graphene were tuned in order to achieve high electrical conductivity.
- Among the composites, CG_3P and CP_5 demonstrated excellent electrochemical performance with maximum specific capacitance of 1519 and 939 Fg^{-1}, respectively.
- The CG_3P composite retained 88% of initial capacitance, indicating excellent cycle life stability.

Development of supercapacitor systems based on binary and ternary nanocomposites using chitosan, graphene and polyaniline

Anand Torvi, Satishkumar Naik, Mahadevappa Kariduraganavar*

Department of Studies in Chemistry, Karnatak University, Pavate Nagar, Dharwad - 580003, Karnataka State, INDIA.

*** Corresponding author address:**

Dr. Mahadevappa Kariduraganavar.
Department of Studies in Chemistry,
Karnatak University, Pavate Nagar,
Dharwad - 580003, Karnataka State, INDIA.

E-mail: *mahadevappayk@gmail.com*

ABSTRACT

Present work describes the preparation of series of binary (chitosan-polyaniline, CP_1 to CP_7) and ternary (chitosan-graphene-polyaniline, CG_1P to CG_5P) composites via *in-situ* polymerization of aniline. The physico-chemical properties of the developed composites were studied. The electrical conductivity of all the composites was measured using four-probe method, and found that among the composites CP_5 and CG_3P composites showed an excellent electrical conductivity as high as 4.165×10^{-1} and 2.9745 S cm^{-1}, respectively. The electrochemical performance was systematically investigated. Electrochemical measurements indicated that the specific capacitance of CG_3P composite was found to be 1519 F g^{-1} at a scan rate of 5 mV s^{-1} in 1 M H_2SO_4 electrolyte solution, which is remarkably higher than those of pure PANI (495 F g^{-1}) and CP_5 (939 F g^{-1}). Further, it is found that 88% of the initial capacitance of CG_3P was retained after repeating 1000 cycles, which demonstrates the excellent cycle life stability.

Graphical Abstract:

Keywords: Supercapacitor, Electrical conductivity, Chitosan, Graphene, Polyaniline.

Specification Table

Subject area	*Polymer chemistry, material science*
Compounds	*Chitosan, graphene, polyaniline*
Data category	*Synthesized, spectral, physicochemical, and electrochemical*
Data acquisition format	*IR, XRD, SEM, TGA, electrochemical characterization, etc.*
Data type	*Analyzed*
Procedure	*Modified Hummers method, reduction, in-situ polymerization*
Data accessibility	*All data are available with this article*

1. Rationale

The increase of environmental pollution and decrease of fossil fuels together prompted the development of sustainable and renewable alternative energy resources while focusing on ways to reduce CO_2 emission [**1,2**]. Now a days, secondary batteries and supercapacitors have gained great attention [**3**]. Supercapacitors also known as electrochemical capacitors have some fascinating features, such as high power density, longer cycle life, short charging time and low maintenance cost. These features make them promising energy storage devices in a wide range of applications, such as portable electronics, hybrid electric vehicles, military devices and memory backup devices **[4-8]**.

To bring the efficient supercapacitors, the development of electrode materials plays a key role. The carbon materials, transition metal oxides and conductive polymers (CP's) have become the most commonly employed electrode materials [**9-12]**. However, each material has its unique advantages and disadvantages for supercapacitor applications. Commonly used conducting polymers in supercapacitors are polyaniline (PANI**) [13,14]** polypyrrole (PPy) **[15-17]** poly(3,4-ethylenedioxythiophene) (PEDOT) **[18]** and poly(o-anisidine) **[19]**. Among

these, PANI is one of the most investigated CP's owing to its facile synthesis, environmental stability, good electrical conductivity and uncommon conducting/insulating fast transition by doping/dedoping process **[20,21]**. Graphene is an outstanding candidate as an electrode material. Graphene sheet is basically a single layer with 2D hexagonal lattice of sp^2 carbon atoms, which are covalently bonded along the two plane directions [**22,23]**. Another outstanding characteristic of graphene is its exceptionally high specific surface area. Unfortunately, the pure form of graphene electrode does not exhibit the desired specific capacitance owing to its inevitable aggregation of graphene sheets **[24]**. Thus, preventing the aggregation of graphene nanosheets is of great importance to improve the properties of graphene based nanocomposites for supercapacitor devices. There are reports, wherein dispersion of graphene in the polymer matrix was improved by covalent and non-covalent modifications of graphene with surfactants **[25,26]**. However, most of the surfactants are toxic and difficult to remove from the composites due to their strong affinity with the graphene surfaces, which limit the application potentiality. Chitosan (CS) can improve the dispersion of graphene in the polymer matrix. Recently, CS and its derivatives have been reported for the modification of graphene to improve their dispersion state effectively **[27]**. Besides, CS also exhibits unique properties, such as biocompatibility, high mechanical strength, low cost, chemical inertness and biodegradability **[28]**. In view of this, hybrid composite materials have been developed based on chitosan with metal oxides, conducting polymers and carbon based materials owing to the excellent properties of individual components and their synergistic effect **[29-37]**.

Understanding the intrinsic properties of aforementioned composites and their electrochemical performances, we have developed the chitosan based binary and ternary nanocomposites in one step by *in-situ* polymerization technique. The physico-chemical properties, electrical conductivity, and electrochemical properties of the resulting series of

composites were studied by employing various techniques. Results were discussed in terms of the individual properties of the components and their synergistic effect.

2. Procedure

2.1. Materials

Aniline purchased from Sigma-Aldrich Chemie, GmbH, Germany was purified by distillation under reduced pressure, Chitosan (M_w 1.86×10^5), graphite flakes (325 mesh) and ammonium persulfate were purchased from S. D. Fine Chemicals Ltd., Mumbai, India. All other reagents used in our experiment were of analytical reagent grade and used without further purification. Deionised (DI) water was used throughout the experiment.

2.2. Methods

2.2.1. Fourier transform infrared (FT-IR) spectroscopy

The interaction between chitosan, reduced graphene oxide and the polyaniline was studied using FT-IR spectrometer (Nicolet, Impact-410, USA). The spectra were recorded in the range of 400–4000 cm^{-1}.

2.2.2. X-Ray diffraction (XRD)

The XRD patterns of all the samples were recorded at room temperature using an X-ray diffractometer (Bruker, D-8 Advance, Germany). The X-ray source was nickel-filtered CuKα radiation (40 KV, 30 mA). The sample was mounted on a sample holder and scanned in the reflection mode at an angle 2θ over a range of 5 to 60^o at a speed of 2^o min^{-1}.

2.2.3. Thermogravimetric analysis (TGA)

The thermal stability of all the samples was assessed using a thermogravimetric analyzer (TA Instruments, DSC Q 20, Waters LLC, USA) at a heating rate of 10 ^oC min^{-1}

under nitrogen atmosphere. The weight of the samples taken for each record was about 8-10 mg.

2.2.4. Scanning electron microscopy (SEM)

The surface morphology of all the samples was recorded using scanning electron microscope (JEOL, JSM-400 Å, Tokyo, Japan). All the samples were sputtered with gold to have good electrical contact and avoid charging.

2.2.5. Electrical conductivity measurements

The electrical conductivity of PANI, and composites such as CP_1 to CP_7 and CG_1P to CG_5P composites were measured with a conventional four-point probe technique (SES Instruments Pvt. Ltd., DF-P-02, India) at 25 ^{o}C. The procedure for the measurement is as follows: 0.5 g of each sample was finely ground in a mortar pestle and pellet was made with the help of a hydraulic pressure of about 400 kg cm^{-2}. The thickness of each pellet was measured using peacock gauge (Ozaki MFG. Co. Ltd, Model G, Japan). The pellet was placed on the base plate of the probe arrangement and the probes were allowed to rest on the middle of the pellet. A gentle pressure was applied on the probes and it was then tightened so as to piercing the sample by the probes. The current was passed through the two outer probes and the floating potential across the inner pair of probes was measured. The same procedure was adopted for the remaining samples.

The current-voltage data measured by a 4-in-line probe dc electrical conductivity instrument were processed for the calculation of resistivity (ρ_o) using the Eq. (1):

$$\rho_0 = \left(\frac{V}{I}\right) \times 2\pi S \qquad (1)$$

where V is the voltage (mV) and I is the current (mA). Since the thickness of the sample was so small as compared to the probe distance, a correction factor was applied and

calculated the corrected resistivity using the Eq. (2):

$$\rho = \frac{\rho_0}{G7\left(\frac{W}{S}\right)} \quad (2)$$

where ρ is the corrected resistivity in ohm cm^{-1}, G7 (W/S) is the correction factor used in case of non-conducting bottom surface, and W is the thickness of the sample (cm) and S is the probe spacing (cm). Thus, the electrical conductivity (σ) was calculated using the Eq. (3):

$$\sigma = {}^{1}/_{\rho} \quad (3)$$

where σ is the electrical conductivity in S cm^{-1}.

2.2.6. Electrochemical measurements

Electrochemical measurements of PANI, and composites such as CP_1 to CP_7 and CG_1P to CG_5P were performed using three-electrode system. The working electrode was a glassy carbon electrode with a diameter of 3 mm. The platinum wire was used as a counter electrode while Ag/AgCl was used as a reference electrode. Typically, 4 mg of sample was initially dispersed with a sonicator in 1 mL of absolute ethanol and to this, 10 µL of polytetrafluoroethylene (PTFE) emulsion (60%) was added. The resulting suspension of 10 µL was dropped onto the glassy carbon electrode using a pipette gun and dried at room temperature. The cyclic voltammetry (CV) study was performed using an electrochemical work station (ACM instrument, GILL AC, USA) at room temperature using 1 M H_2SO_4 as an electrolyte. The CV measurements were carried out from -1 to +1 V at various scan rates of 5-120 mV s^{-1}. Cycle life stability of the samples was tested at fixed scan rate of 50 mV s^{-1} for 1000 cycles.

2.3. Synthesis

2.3.1. Synthesis of binary chitosan-polyaniline (CP) composites

The chitosan-polyaniline (CP) binary composites were prepared by following the method as described here. First, the chitosan solution was prepared by dissolving 0.5 g of chitosan powder in 2 wt% of aqueous acetic acid solution and stirred overnight to get a homogenous solution. To this chitosan solution, 5×10^{-3} M aniline monomer was added and allowed for stirring. After 30 minutes, a calculated amount of ammonium persulfate solution prepared in 0.5 M HCl was added as an oxidant. Upon addition of ammonium persulfate, colour of the solution slowly turned green, which confirmed the polymerization of aniline. While stirring, the reaction was kept overnight to complete the polymerization. Subsequently, the reaction mixture was neutralized by the addition of 5% NaOH solution and the resulting graft copolymer was precipitated by adding an adequate quantity of ethanol. The precipitate thus obtained was washed with N-methyl pyrrolidine (NMP) and followed by acetone. Finally, the product was dried for 2 days in a vacuum oven at 55 ^{o}C. The compound was designated as CP_1. Similarly, other composites (CP_2 to CP_7) were prepared by varying the concentration of aniline monomer. The molar ratio of oxidant to monomer was 1.2:1. The pure PANI was also prepared to compare the results.

2.3.2. Synthesis of ternary chitosan-reduced graphene oxide-polyaniline (CGP) composites

Fig. 1. Illustration of the experimental procedure for the synthesis of CGP nanocomposites by *in-situ* polymerization.

The ternary CGP composite was synthesized via *in-situ* chemical oxidation of aniline monomer in the presence of chitosan-graphene template. Chitosan (0.5 g) was dissolved in 2 wt% of acetic acid solution and stirred overnight at room temperature to obtain homogenous solution as shown in Fig. 1(a). To this, a known amount of reduced graphene oxide (RGO) was added and subjected to sonication for 20 minutes [Fig. 1(b)]. The rest of the polymerization procedure was followed as similar to the procedure adopted for the preparation of binary CP composites. However, the concentration of aniline and ammonium

persulfate was fixed as similar to CP_5 composite and varied the amount of the RGO as shown in Fig. 1(c). The resulting hybrid ternary composites were designated as CG_1P to CG_5P depending on the content of RGO.

3. Data, value and validation

3.1. FT-IR study

Fig. 2. Illustration of FT-IR spectra of CS, PANI, CP_5, CG_3P and RGO.

The FTIR spectra of pure chitosan, PANI, RGO, binary composite CP_5 and ternary composite CG_3P are shown in Fig. 2. The spectrum of pure chitosan exhibited a strong and broad band at around 3400 cm^{-1}**,** which is attributed to the stretching vibrations of both –NH and –OH groups. The bands appeared at 1659 and 1597 cm^{-1} are respectively assigned to amino-I and amino-II groups of chitosan **[38]**. The multiple bands observed between 1000 and 1200 cm^{-1} are assigned to C-O stretchings. In the FT-IR spectrum of pure PANI, the characteristic bands observed at 1565 and 1486 cm^{-1} are respectively assigned to C=C stretchings of quinonoid and benzenoid rings **[39,40]**. The bands at 1298 and 1245 cm^{-1} are attributed to the stretching vibrations of C-N and C=N, respectively **[41,42]**. The FTIR spectrum of CP_5 showed characteristic peaks of PANI as well as chitosan. However, the band observed at 1083 cm^{-1} in the CS spectrum was shifted slightly to higher wavelength of 1109 cm^{-1}. All these evidences ascertain the formation of PANI and its grafting onto chitosan. In the FT-IR spectrum of RGO, the band appeared at 1571 cm^{-1} corresponds to C=C stretchings, indicating that graphene oxide underwent reduction. The stretching vibrations appeared in the CG_3P and CP_5 are closed to each other. This result demonstrates interaction between CS, RGO and PANI.

3.2. XRD study

Fig. 3. XRD pattern of CS, PANI, CP_5, RGO and CG_3P.

The X-ray diffraction patterns of pure CS, PANI, RGO, and composites such as CP_5 and CG_3P are shown in Fig. 3. The pattern of chitosan showed a sharp peak centered at $2\theta = 20^o$, suggesting that chitosan is dominated by the crystalline nature [**43,44**]. The PANI exhibited several peaks, with the intense peak at $2\theta = 25.5^o$. These reflections indicate some crystalline order in the bulk of PANI sample **[39]**. In XRD pattern of CP_5, the two peaks were observed at $2\theta = 20^o$ and 25.8^o, which respectively correspond to CS and PANI. This confirms that PANI is successfully grafted onto CS. Pure RGO exhibited a broad reflection peak centered at $2\theta = 24.5^o$, revealing high reduction of GO and the exfoliation of the layered RGO **[45].** This is clearly observed in the SEM images of reduced graphene oxide. The XRD pattern of CG_3P composite is almost similar to the pattern of CP_5. This infers that the RGO sheets are so weak, and thus they are overlapped with the chains of PANI. This further reveals that most of the RGO sheets were exfoliated and uniformly dispersed in the polymer matrix.

3.3. TGA study

Fig. 4. Thermograms of CS, PANI, RGO and composites CP_5 and CG_3P.

The thermal stability and degradation behaviour of chitosan, PANI, RGO and their composites were investigated under nitrogen atmosphere using TGA and the resulting thermograms are shown in Fig. 4. Chitosan, PANI, RGO and their composites showed the weight loss of about 10-16% in the temperature range of 60-110 ^oC. This is due to the loss of adsorbed water molecules. In the second stage, weight loss of chitosan started at around 280 ^oC, that corresponds to the loss of polymeric chains, while the decomposition of binary CP_5 and ternary CG_3P composites occurred between 120 and 250 ^oC, and is attributed to the weight loss of PANI **[31,34]**. The weight loss of CP_5 and CG_3P after 250 ^oC was mainly due to the degradation of the polymer backbone [**31].** The thermal stability of binary CP_5 is increased by the addition of PANI, and the thermal stability of ternary CG_3P composites is

increased due to the RGO content. The TGA pattern of reduced graphene oxide (RGO) exhibited weight loss of around 31% up to the measured temperature (800 ^{o}C). This is mainly due to the reduction of oxygen containing functional groups. Similarly, the pure PANI exhibited mass loss of around 66% in the temperature range of 100 to 800 ^{o}C. Further, it is observed that still there is 30, 38 and 43 mass% of residue weights remained at 800 ^{o}C in chitosan, CP_5 and CG_3P, respectively. The highest mass% of residue (43%) is observed in CG_3P composite as compared to CP_5 and CS, which indicates that ternary composite exhibited good thermal stability. This is obviously because of the incorporation of RGO into CP matrix.

3.4. Surface morphology

Fig. 5. SEM images of PANI (a,b), CP_5 (c,d), RGO (e,f) and CG_3P (g,h) with different magnifications.

The surface morphology of CS, PANI, RGO, and composites of CP_5 and CG_3P was shown in Fig. 5. The PANI has shown short rod like nanofibers (Fig. 5.a,b). After the incorporation of PANI into chitosan, the resulting binary composite CP_5 showed morphology like roots of the tree spread over the land in the low magnification of SEM images (inlet colour image, Fig. 5 c). However, magnified image (Fig. 5 d) has shown the surface having short rod like fibrous structure accumulated with granular form of polyaniline. The RGO has shown sheet like morphology in the images, which confirms the high degree of reduction (Fig. 5 e,f). From the SEM images of CG_3P composite (Fig. 5 g,h), it is observed that small granule shaped PANI randomly attached on the surface of well dispersed conducting RGO (denoted by yellow coloured arrow). The coating of PANI over the graphene plates can easily perceived by comparing the SEM images of CG_3P composite and pure RGO. Here, the PANI did not coat on the full surface of RGO since it is mainly in the form of granules or fibre like structure, yet it was mostly covered the surface with its granule structure. The adherence of

granule shaped PANI over the RGO formed a conducting network in the CG_3P composite and established the π–π interactions among them. Similar conclusions were drawn by Kumar et al. **[46]**. Due to this reason, the CG_3P ternary composite demonstrated the highest specific capacitance. Further, this coating and intercalations inhibit the restacking of individual graphene layer owing to severe Van der Waals force of attraction among them.

3.5. Electrical conductivity study

Table 1 Electrical conductivity of samples CP_1 to CP_7, CG_1P to CG_5P, pure PANI and RGO.

The electrical conductivity of pure PANI, RGO, binary composites CP_1 to CP_7 and ternary composites CG_1P to CG_5P was measured using a four-point probe method and data are presented in Table 1. In order to achieve the highest electrical conductivity, the reaction protocol was tuned by varying the aniline concentration with constant mass of chitosan. As the concentration of aniline was increased, the electrical conductivity increased initially from CP_1 to CP_5 with a maximum electrical conductivity of about 4.165×10^{-1} S cm^{-1}, and then decreased for CP_6 and CP_7. This is because, the further addition of aniline into the chitosan matrix was lead to the formation of aggregates, which resisted the transport of effective charge along the conductive networks and thereby the electrical conductivity was decreased. Among the binary composites developed here, CP_5 exhibited the highest electrical conductivity of 4.165×10^{-1} S cm^{-1}, which is higher than those of chitosan based binary composites reported by Tiwari et al. **[47]** and Yuvaz et al. **[31].** Further to increase the electrical conductivity of CP_5, we have varied the amount of RGO.

As similar to binary composites, electrical conductivity of the ternary composites was increased with increasing the mass% of RGO and reached maximum electrical conductivity of 2.9745 S cm^{-1} for CG_3P and then decreased with further increasing the mass% of RGO. The decrease in electrical conductivity for CG_4P and CG_5P is due to the formation of isolated

aggregates, which hindered the transport of charge along the conductive network as noticed in the binary composites **[48,49]**. Thus, the CG_3P ternary composite demonstrated the highest electrical conductivity and is much higher than those of RGO and PANI. This is mainly due to the formation of nanostructure in the ternary composite and the synergistic effects resulted from three components. Firstly, the addition of plate like structure of graphene greatly improved the electrical conductivity due to the formation of conductive networks for the charge transport throughout the insulating chitosan polymer matrix. Secondly, the π-π stacking between the PANI polymer backbone and the RGO sheets further enhanced the electrical conductivity of the ternary composite. The specific capacitance determined for the series of binary and ternary composites also supported the electrical conductivity behaviour, since electrical conductivity is one of the prime requirements for achieving the high specific capacitance.

3.6. Electrochemical performance

Fig. 6. Cyclic voltammograms of PANI, CP_5 and CG_3P measured in three-electrode system with a potential range of -1to +1 V in 1 M H_2SO_4 electrolyte solution at different scan rates of 5-120 mV s^{-1} (a-c); Cyclic voltammograms of PANI, CP_5 and CG_3P measured at a fixed scan rate of 5 mV s^{-1} (d).

Figure 6 (a, b and c) shows the CV curves of PANI, CP_5 and CG_3P measured at different scan rates of 5-120 mV s^{-1} in 1 M H_2SO_4 solution. It is found that the peak current in the CV curves was slowly increased with scan rate. This indicates that the CV current is directly proportional to the scan rate. The cyclic voltammograms at high scan rates did not show sharp redox peaks over the potential range. This is because of the slow kinetics of the redox reaction of the electrode as well as the limited proton diffusion migration as compared to the low scan rate **[50]**.

Figure 6d shows the CV curves of PANI, CP_5 and CG_3P performed at fixed scan rate of 5 mV s^{-1} in 1 M H_2SO_4 solution. All the CV curves exhibited two pairs of redox peaks (C_1/A_1, C_2/A_2), which are the indicative of typical pseudocapacitive characteristic of PANI. The peaks C_1/A_1 are related to the redox transitions of PANI from a semiconducting state (leucoemeraldine form) to a conducting state (emeraldine form). The Peaks C_2/A_2 are corresponds to Faradaic transformations from emeraldine to pernigraniline **[51-53]**. The redox peaks of CP_5 exhibited higher current than that of pure PANI and lower current than that of CG_3P. Since there is a linear relation between CV area and the specific capacitance, the CG_3P composite exhibited higher specific capacitance than those of CP_5 and PANI. The electrochemical performance was also conducted for other binary and ternary composites under the same condition and the CV curves are given as supplementary information in Figs. S1 and S2.

The specific capacitance was calculated from the CV curves according to the Eq. 4 **[54-56]**.

$$C_{sp} = \frac{\int Idv}{\Delta V.s.m} \qquad (4)$$

where C_{sp} is the specific capacitance (F g^{-1}), Idv is the integrated area under the CV curve, m is the mass of active material deposited on the electrode surface (mg), ΔV is the difference in potential (V), and s is the potential scan rate (mV s^{-1}). The specific capacitance of PANI, binary composite (CP_5), ternary composite (CG_3P) were respectively found to be 495, 939, and 1519 F g^{-1}. Among the three components studied here, the CG_3P demonstrated an excellent electrochemical performance and is mainly due to high electrical conductivity, well-designed nanostructure and their synergistic effects. Firstly, the addition of graphene can greatly improve the electrical conductivity. Secondly, the presence of PANI can remarkably increase the pseudo-capacitance contribution to the overall capacitance. Lastly, the presence

of highly polarizable substituents of chitosan, such as amino (-NH_2) and hydroxyl (-OH) groups greatly reduces, the ionic transfer resistance at the electrode–electrolyte interface and improve EDLC high-rate performance **[57]**. In addition, Chitosan prevents the aggregation of graphene nanosheets and provides the high specific capacitance. Similar conclusions were made by Lu et al. **[58]** and Pandiselvi et al. **[34]** The cyclic voltammograms of CG_3P demonstrates the combination of both redox capacitance and EDLC. Furthermore, the incorporation of RGO in the composite offers high conductive path and also serves as a high surface area support material for the polymerization of PANI, thereby facilitates the rapid transport of electrolyte ions in the electrode during rapid charge/discharge processes. All these are responsible for the overall improvement of electrochemical properties of CG_3P ternary nanocomposite.

Fig. 7. Variation of the specific capacitance of PANI, CP_5 and CG_3P at different scan rates of 5-120 mV s^{-1} (a); Nyquist plots of PANI, CP_5 and CG_3P (b); Variation of the specific capacitance at different concentration of PANI (c), mass% of RGO (d).

Figure 7a depicts the relation between specific capacitance and the scan rates of pure PANI, CP_5 and CG_3P. The specific capacitance of CG_3P composite is much higher than those of pure PANI and binary CP_5 composite. The maximum specific capacitance of 1519 F g^{-1} is obtained at a scan rate of 5 mV s^{-1} for CG_3P, as compared to 939 and 495 F g^{-1} for CP_5 and PANI, respectively. Even at 120 mV s^{-1}, the CG_3P exhibited higher specific capacitance of 465 F g^{-1}, while CP_5 and PANI respectively showed only 247 and 148 F g^{-1}. The variation in the specific capacitance of series of binay CP and ternary CGP composites is shown in Fig. 7 (c,d). The specific capacitance achieved for CG_3P composite is much higher than those reported for chitosan and PANI based composites. For instance, Pandiselvi et al. **[34]** developed CS-ZnO-PANI composite and obtained a maximum specific capacitance of (587 F g^{-1}). Hassan et al. **[32]** obtained the highest specific capacitance of 424 F g^{-1} for MnO_2-

chitosan hybrid nanocomposite film. Dorrajji et al. **[33]** reported maximum capacitance of 14.48 F cm^{-2} for polyaniline-MWCNT nanocomposite synthesized on the surface of chitosan wet-spun fibers. Similarly, the CS–SnO_2–PANI modified electrode exhibited the specific capacitance of about 179.20 F g^{-1} in 1 M H_2SO_4 solution at 10 mV s^{-1} **[37]**.

Electrochemical impedance spectroscopy (EIS) is another technique, which is complementary to galvanostatic measurement, and provides more information on the electrochemical behaviour of the system, and thus one can obtain an equivalent series resistance (ESR). Accordingly, EIS measurements were carried out with a frequency range of 0.1 Hz-30 kHz at fixed amplitude of 10 mV. The EIS data were analyzed by plotting the real (Z') and imaginary (Z″) parts of the impedance data of PANI, CP_5 and CG_3P composite electrodes as shown in Fig. 7b. These plots are usually called cole-cole or Nyquist plots. In all the curves, the lower left portion of the curves corresponds to the higher frequencies. Thus, higher the vertical curve better is the closeness towards ideal capacitor of the electrode **[59]**. The ESR of the electrode can be drawn from the X-intercept of the Nyquist plot. All the materials developed here have shown comparable low ESR of about 2-4 Ω. No samples exhibit semicircles in the high-frequency region. This is because of low Faradaic resistance of the electrode material. Among the samples, CG_3P has shown more vertical line towards imaginary axis, and thereby suggests a better capacitive nature. This is mainly attributed to the incorporation of conductive graphene into chitosan-polyaniline template. The presence of inclined line at low frequency could be attributed to the diffusion limitation of ions (SO_4^{-2}) in the active materials (PANI) which is often referred as Warburg impedance **[33]**. From the plots, it is observed that the difference in slope at low frequency is attributed to the incorporation of conductive graphene in the formation of composite with high porosity. This is more predominant in case of CG_3P as expected. This is very well supported by the SEM images as shown in Fig. 5 (g,h).

Fig. 8. Galvanostatic charge-discharge curves of the CG_3P, CP_5 and PANI composite electrodes.

The galvanostatic charge-discharge (GCD) study was carried out using electrochemical works station (CH Instruments Inc., CHI 608E, USA) over a potential range of -1 to +1 V and the current density was fixed at 0.1 A g^{-1}. The galvanostatic charge–discharge is a consistent method to determine the electrochemical performance of materials. The charge-discharge behaviour of PANI, CP_5 and CG_3P composite materials is shown in Fig. 8. The GCD curves are not symmetrical and shown a deviation from the triangular shape, suggesting that the developed electrode exhibited the redox behaviour. This might be due to a pseudocapacitance contributed from the Faradaic reaction of polyaniline. When the potential was reversed, the total impedance of the cell gave rise to an initial IR drop (potential drop) during the discharge process. The potential drop for the CG_3P composite electrode is smaller as compared to the CP_5, and PANI electrode. This result suggests that the internal resistance of the CG_3P composite is smaller than the CP_5, and PANI. The specific capacitance was estimated using the Eq. (5):

$$C_S = \frac{I\Delta t}{m\Delta V} \qquad (5)$$

where C_s is specific capacitance, 'I' is the discharge current, 'Δt', the discharge time, 'm' is the mass of the active material, and 'ΔV' is the potential window. According to the above equation, the specific capacitance of CG_3P electrode (1326.82 F g^{-1}) is more than that of CP_5 (591.37 F g^{-1}) and PANI (295.48 F g^{-1}). The results infer that the CG_3P nanocomposite exhibits a good capacitive behaviour under same current density, which is in good agreement with the result obtained from CV curves.

Table 2 Comparison of specific capacitance of the developed composite electrode materials with the reported PANI based composite materials.

The specific capacitance of PANI and its composites measured at a fixed current density of 0.1 A g^{-1} using two/three electrode system in different electrolytes are summarized in Table 2. It is observed that specific capacitances of pure PANI and ternary composite CG_3P were found to be 296 and 1327 F g^{-1}.

Among the composite materials reported previously, the ternary composite material KSC/CNT/PANI and binary composite material M-GR/PANI demonstrated an excellent specific capacitance of 1090 and 1118 F g^{-1}, respectively. These specific capacitance values are much lower than the ternary composite material (CG_3P) developed in the present study. This clearly signifies that the ternary composite material (CG_3P) developed by judiciously varying the amount of chitosan, PANI and RGO yielded the highest specific capacitance among the PANI based composites reported **[60-69]**.

Fig. 9. Cycle life stability of PANI, CP_5 and CG_3P at fixed scan rate of 50 mV s^{-1}.

The cycle-life test of the pure PANI, CP_5 and CG_3P electrodes was performed for 1000 cycles at a scan rate of 50 mV s^{-1}. From the Fig. 9, it is observed that the specific capacitance of CG_3P decreases from 635 to 579 F g^{-1} in the initial 400 cycles and this corresponds to 91% of its initial value, then levels off gradually in the following cycles, and finally 88 % of specific capacitance is retained after 1000 cycles. It is inferred that the partial structural damage or detachment of PANI nanofibers occurs over the initial 400 cycles and leads to decay in specific capacitance. Subsequently, the structure tends to be stable, resulting in an approximately stable capacitance in the following cycles. On the contrary, the CP_5 nanocomposite has retained 69% of specific capacitance of its initial value. The capacitance of pure PANI continues to decrease throughout the cycling process, the capacitance decreased from 175 to 91 F g^{-1}, which corresponds to 52% of its initial value. When we compare the retention capacity between pure PANI and CP_5, the binary CP_5 composite has shown higher value (69%) than that of pure PANI (52%). This is because, during the cycle-

life test, the doping or dedoping of H^+ into or from the PANI chains results in the swelling and shrinkage of the nanostructured conducting polymer **[53]**. However, this was greatly increased the cycle stability after the grafting of PANI with CS. This dramatically reduced the swelling and shrinkage property of PANI during the doping/dedoping processes **[70]**. The improved cycling stability of CG_3P composite can be attributed to the embedding of chemically grafted graphene, the elastic graphene with rich wrinkles can act as elastic network alleviating the irreversible structural damages of PANI or falling off from electrode, thus maintains a high cycling stability.

4. Conclusion

In summary, a series of composites of CP_1 to CP_7 and CG_1P to CG_5P were developed by *in-situ* polymerization of aniline. The molar ratio of aniline and mass ratio of graphene were tuned in order to achieve high electrical conductivity. Among the series of composites, CP_5 and CG_3P demonstrated an excellent electrical conductivity of 4.165×10^{-1} and 2.9745 S cm^{-1}, respectively. This is due to an establishment of conductive network from the polyaniline and reduced graphene oxide. From the thermal study, it is revealed that the composites are stable up to 800 ^oC. The developed composites particularly CP_5 and CG_3P demonstrated an excellent electrochemical performance with maximum specific capacitance of 939 and 1519 F g^{-1}, respectively. In addition, CG_3P and CP_5 respectively exhibited 88 and 69% retention of initial capacitance over 1000 cycles. The enhanced cycle-life performance of CG_3P composite is mainly attributed to synergistic effect occurred between three individual components. Meanwhile, the electrodes made of CP_5 and CG_3P exhibited excellent specific capacitance among the composites developed. Thus, these two electrodes could be used to develop high performance, environmentally friendly and low cost electric energy storage devices.

Abbreviations

CGP	Chitosan-graphene-polyaniline
FT-IR	Fourier transform infrared spectroscopy
XRD	X-Ray diffraction
TGA	Thermogravimetric analysis
CV	Cyclic voltammetry
EDLC	Electrical double-layer capacitors
CP	Conductive polymers
ESR	Equivalent series resistance
PTFE	Polytetrafluoroethylene
RGO	Reduced graphene oxide
PANI	Polyaniline
MWCNT	Multiwalled carbon nanotube
V	Potential window
S	Potential scan rate
W	Thickness of the sample
S	Probe spacing
σ	Electrical conductivity

Acknowledgments

The authors thank the UGC, New Delhi, for providing the financial support under CPEPA program [Grant No. 8-2/2008(NS/PE)]. This work is also supported by the DST-PURSE-Phase-II program, Department of Science & Technology, New Delhi, [Grant No. SR/PURSE PHASE-2/13(G)].

Declaration of interest

Declarations of interest: none

Supplementary materials

The preparation of graphene oxide and reduced graphene oxide (RGO). Electrochemical performance of binary CP_1 to CP_7 (except CP_5) and ternary CG_1P to CG_5P (except CG_3P) composite. Thickness measurement of RGO by atomic force microscopy.

References

[1] C. Liu, F. Li, L. Ma, H. Cheng, Advanced materials for energy storage, Adv. Mater. 22 (2010) E28–E62.

[2] J.R. Miller, P. Simon, Electrochemical capacitors for energy management, Science 321

(2008) 651–652.

[3] P. Simon, Y. Gogotsi, Materials for electrochemical capacitors, Nat. Mater. 7 (2008) 845–854.

[4] J.A. Lee, M.K. Shin, S.H. Kim, H.U. Cho, G.M. Spinks, G.G. Wallace, M.D. Lima, X. Lepro, M.E. Kozlov, R.H. Baughman, S.J. Kim, Ultrafast charge and discharge biscrolled yarn supercapacitors for textiles and microdevices, Nat. Commun. 4 (2013) 1907.

[5] D. Hulicova, M. Kodama, H. Hatori, Electrochemical performance of nitrogen enriched carbons in aqueous and non-aqueous supercapacitors, Chem. Mater. 18 (2006) 2318.

[6] M. Winter, R.J. Brodd, What are batteries, fuel cells, and supercapacitors? Chem. Rev. 104 (2004) 4245.

[7] S. Jayalexmi, A. Puthirath, Supercapacitors: Fundamental aspects, in: A. Blakrishan, K.R.V. Subramanian (Eds), Nanostructured ceramic oxides for supercapacitor applications, CRC press, Boca Raton, 2014, pp. 41.

[8] V. Gupta, N. Miura, Polyaniline/single-wall carbon nanotube (PANI/SWCNT) composites for high performance supercapacitors, Electrochim. Acta 52 (2006) 1721.

[9] E. Frackowiak, Carbon materials for supercapacitor application, Phys. Chem. Chem. Phy. 9 (2007) 1774.

[10] C.C. Hu, K.H. Chang, M.C. Lin, Y.T. Wu, Design and tailoring of the nanotubular arrayed architecture of hydrous RuO_2 for next generation supercapacitors, Nano Lett. 6 (2006) 2690.

[11] H. Zhou, H.‑J. Zhai, An effective approach to prepare three-dimensional porous manganese dioxide electrodes by surfactant assisted electrosynthesis for improved supercapacitive properties, J Mater Sci: Mater Electron. 28 (2017) 13983–13989.

[12] H. Wang, H.S. Casalongue, Y. Liang, H. Dai, $Ni(OH)_2$ nanoplates grown on graphene

as advanced electrochemical pseudocapacitor materials, J. Am. Chem. Soc. 132 (2010) 7472.

[13] S. Bhadra, D. Khastgir, N.K. Singha, J.H. Lee, Progress in preparation, processing and applications of polyaniline, Prog. Polym. Sci. 34 (2009) 783.

[14] M. Manoj, K.M. Anilkumar, B. Jinisha, S. Jayalekshmi, Polyaniline-graphene oxide based ordered nanocomposite electrodes for high-performance supercapacitor applications, J Mater Sci: Mater Electron. 28 (2017) 14323–14330.

[15] H. Zhou, H.‐J. Zhai, Boosting the electrochemical capacitive properties of polypyrrole using carboxylated graphene oxide as a new dopant, J Mater Sci: Mater Electron. 29 (2018) 7893–7903.

[16] H. Zhou, Optimized preparation of core–shell composites based on polypyrrole doped with carbon nanotubes for high performance electrochemical capacitors, J Mater Sci: Mater Electron. 29 (2018) 7857–7866.

[17] A.I. Torvi, B.B. Munavalli, S.R. Naik, M.Y. Kariduraganavar, Scalable fabrication of a flexible interdigital micro-supercapacitor device by in-situ polymerization of pyrrole into hybrid PVA-TEOS membrane, Electrochimica Acta 282 (2018) 469-479.

[18] H. Zhou, H.–J. Zhai, G. Han, Adjust the electrochemical performances of graphene oxide nanosheets-loaded poly(3,4-ethylenedioxythiophene) composites for supercapacitors with ultralong cycle life, J Mater Sci: Mater Electron. 27 (2016) 2773–2782.

[19] R. Ojani, J. Raoof, S. Zamani, A novel sensor for cephalosporins based on electrocatalytic oxidation by poly (o-anisidine)/SDS/Ni modified carbon paste electrode, Talanta 81 (2010) 1522–1528.

[20] K.R. Reddy, W. Park, B.C. Sin, J. Noh, Y. Lee, Synthesis of electrically conductive and superparamagnetic monodispersed iron oxide-conjugated polymer composite

nanoparticles by *in-situ* chemical oxidative polymerization, J. Colloid Interface Sci. 335 (2009) 34–39.

[21] J. Yan, T. Wei, B. Shao, Z. Fan, W. Qian, M. Zhang, F. Wei, Preparation of a graphene nanosheet/polyaniline composite with high specific capacitance, Carbon 48 (2010) 487-493.

[22] K.S. Novoselov, A.K. Geim, S. Morozov, D. Jiang, Y. Zhang, S. Dubonos, I. Grigorieva, A. Firsov, Electric field effect in atomically thin carbon films, Science 306 (2004) 666.

[23] C, Lee, X. Wei, J.W. Kysar, and J. Hone, Measurement of the elastic properties and intrinsic strength of monolayer graphene, Science 321 (2008) 385.

[24] A. Esfandiar, O. Akhavan, A. Irajizad, Melatoninas a powerful bio-antioxidant for reduction of graphene oxide, J. Mat. Chem. 21 (2011) 10907.

[25] M. Lotya, Y. Hernandez, P.J. King, Liquid phase production of graphene by exfoliation of graphite in surfactant/water solutions, J. Am. Chem. Soc. 131 (2009) 3611−3620.

[26] Y. Ge, J.L. Wang, Z.X. Shi, J. Yin, Gelatin-assisted fabrication of water-dispersible graphene and its inorganic Analogues, J. Mater. Chem. 22 (2012) 17619−17624.

[27] X.Y. Qiu, Y.H. Yang, L.P. Wang, S.L. Lu, Z.Z. Shao, X. Chen, Synergistic interactions during thermosensitive chitosan-betaglycerophosphate hydrogel formation, RSC Adv. 1 (2011) 282−289.

[28] Y.Z. Pan, H.Q. Bao, L. Li, Non covalently functionalized multiwalled carbon nanotubes by chitosan-grafted reduced graphene oxide and their synergistic reinforcing effects in chitosan films, ACS Appl. Mater. Interfaces 3 (2011) 4819−4830.

[29] S. Anandhavelu, S. Thambidurai, Effect of annealing temperature on optical and electrochemical properties of chitosan–ZnO nanostructure, Ionics 19 (2013) 903– 909.

[30] S. Anandhavelu, S. Thambidurai, Preparation of chitosan–zinc oxide complex during

chitin deacetylation, Carbohydr. Polym. 83 (2011) 1565–1569.

[31] A.G. Yavuz, A. Uygun, V.R. Bhethanabolta, Substituted polyaniline-chitosan composites: synthesis and characterization, Carbohydr. Polym. 75 (2009) 448–453.

[32] S. Hassan, M. Suzuki, A. El-Moneim, Synthesis of MnO_2-chitosan nanocomposite by one-step electrodeposition for electrochemical energy storage application, J. of Power Sources 246 (2014) 68-73.

[33] M.S. Seyed Dorraji, I. Ahadzadeh, M.H. Rasoulifard, Chitosan-polyaniline-MWCNT nanocomposite fibers as an electrode material for electrical double layer capacitors, Int. J. Hydrogen Energy 39 (2014) 9350-9355.

[34] K. Pandiselvi, S. Thambidurai, Chitosan-ZnO-polyaniline hybrid composites: polymerization of aniline with chitosan-ZnO for better thermal and electrical property, Polym. Degrad. Stab. 98 (2013) 988-996.

[35] Y.N. Sudhakar, M. Selvakumar, Lithium perchlorate doped plasticized chitosan and starch blend as biodegradable polymer electrolyte for supercapacitors, Electrochim. Acta 78 (2012) 398-405.

[36] M. Yamagata, K. Soeda, S. Ikebe, S. Yamazaki, M. Ishikawa, Chitosan-based gel electrolyte containing an ionic liquid for high-performance non aqueous supercapacitors, Electrochim. Acta 100 (2013) 275–280.

[37] M. Karpuraranjith, S. Thambidurai, Twist fibrous structure of CS–SnO_2–PANI ternary hybrid composite for electrochemical capacitance performance, RSC Adv. 6 (2016) 40567–40576.

[38] S.K. Choudhari, A.A. Kittur, S.S. Kulkarni, M.Y. Kariduraganavar, Development of novel blocked diisocyanate crosslinked chitosan membranes for pervaporation separation of water–isopropanol mixtures, J. Membr. Sci. 302 (2007) 197–206.

[39] H. Jiu, C. Huang, L. Zhang, J. Chang, H. Jiao, S. Zhang, W.B. Jia, Excellent

electrochemical performance of graphene–polyaniline hollow microsphere composite as electrode material for supercapacitors, J Mater Sci: Mater Electron. 26 (2015) 8386–8393.

[40] N. Arsalani, A.G. Tabrizi, L.S. Ghadimi, Novel PANI-$MnFe_2O_4$ nanocomposite for low-cost supercapacitors with high rate capability, J Mater Sci: Mater Electron. 29 (2018) 6077–6085.

[41] H. Heydari, M.B. Gholiv, Polyaniline-reduced graphene oxide–cobalt sulfide ternary composite for high-performance supercapacitors, J Mater Sci: Mater Electron. 28 (2017) 3607–3615.

[42] H. Mahdavi, P.K. Kahriz, H.G.-Ranjbar, T. Shahalizade, Synthesis and performance study of amino functionalized graphene aerogel grafted with polyaniline nanofibers as an efficient supercapacitor material, J Mater Sci: Mater Electron. 28 (2017) 4295–4305.

[43] Q. Chen, A. Xu, Z. Li, J. Wang, S. Zhang, Influence of anionic structure on the dissolution of chitosan in 1-butyl-3-methylimidazolium-based ionic liquids, Green Chem. 13 (2011) 3446-3452.

[44] Z. Abdeen, S.G. Mohammad, Study of the adsorption efficiency of an eco-friendly carbohydrate polymer for contaminated aqueous solution by organphosphorus pesticide, Open Journal of Organic Polymer Materials 4 (2014) 16-28.

[45] L. Tang, Z. Yang, F. Duan, M. Chen, Hierarchical architecture of ultrashort carbon nanotubes-polyaniline nanocables coated on graphene sheets for advanced supercapacitors, J Mater Sci: Mater Electron. 28 (2017) 15804–15818.

[46] A.K. Das, S.K. Karan, B.B. Khatua, Graphene-polyaniline nanofiber composites as supercapacitor electrodes high energy density ternary composite electrode material based on polyaniline (PANI), molybdenum trioxide (MoO_3) and graphene nanoplatelets (GNP) prepared by sono-chemical method and their synergistic contributions in

superior supercapacitive performance, Electrochim. Acta 180 (2015) 1–15.

[47] A. Tiwari, V. Singh, Synthesis and characterization of electrical conducting chitosan-graft-polyaniline (CS-G-PANI), Express Polymer Lett. 5 (2007) 308–317.

[48] X. Wang, H. Bai, Z. Yao, A. Liu, G. Shi, Electrically conductive and mechanically strong biomimetic chitosan/reduced graphene oxide composite films, J. Mater. Chem. 20 (2010) 9032–9036.

[49] X. Wang, M. Song, Toughening of polymers by graphene, Nanomaterials and Energy 2 (2015) 265–278.

[50] P.R. Deshmukh, R.N. Bulakhe, S.N. Pusawale, S.D. Sartaleb, C.D. Lokhande, Polyaniline–RuO_2 composite for high performance supercapacitors: chemical synthesis and properties, RSC Adv. 5 (2015) 28687.

[51] Y.G. Wang, H.Q. Li, Y.Y. Xia, Ordered whiskerlike polyaniline grown on the surface of mesoporous carbon and its electrochemical capacitance performance, Adv. Mater. 18 (2006) 2619–2623.

[52] Y. Li, X. Zhao, Q. Xu, Q. Zhang, D. Chen, Facile preparation and enhanced capacitance of the polyaniline-sodium alginate nanofiber network for supercapacitors, Langmuir 27 (2011) 6458–6463.

[53] H. Fei, N. Saha, N. Kazantseva, T. Babkova, M. Machovsky, G. Wang, H. Bao, P. Saha, Polyaniline-reduced graphene oxide hydrogel film with attached graphite current collector for flexible supercapacitors, J Mater Sci: Mater. Electron. 29 (2018) 3025–3034.

[54] I. Shakir, High energy density based flexible electrochemical supercapacitors from layer-by-layer assembled multiwall carbon nanotubes and graphene, Electrochim. Acta 129 (2014) 396-400.

[55] L. Qian, L. Lu, Fabrication of three-dimensional porous graphene–manganese dioxide

composites as electrode materials for supercapacitors, Colloids Surf. A 465 (2015) 32-38.

[56] K.M. Anilkumar, M. Manoj, B. Jinisha, V.S. Pradeep, S. Jayalekshmi, Mn_3O_4-reduced graphene oxide nanocomposite electrodes with tailored morphology for high power supercapacitor applications, Electrochim. Acta 236 (2017) 424-433.

[57] K. Pandiselvi, S. Thambidurai, Chitosan-ZnO-polyaniline ternary nanocomposite for high-performance supercapacitor, Ionics 20 (2014) 551–561.

[58] X. Lu, H. Dou, C. Yuan, S. Yang, L. Hao, F. Zhang, L. Shen, L. Zhang, X. Zhang, Polypyrrole-carbon nanotube nanocomposite enhanced the electrochemical capacitance of flexible graphene film for supercapacitors, J. Power Sources 197 (2012) 319-324.

[59] K. Zhang, L.L. Zhang, X.S. Zhao, J. Wu, Graphene-polyaniline nanofiber composites as supercapacitor electrodes, Chem. Mater. 22 (2010) 1392–1401.

[60] X. Lu, H. Dou, S. Yang, L. Hao, L. Zhang, L. Shen, F. Zhang, X. Zhang, Fabrication and electrochemical capacitance of hierarchical graphene-polyaniline-carbon nanotube ternary composite film, Electrochimica Acta 56 (2011) 9224–9232.

[61] F. Chen, P. Liu, Q. Zhao, Well-defined graphene-polyaniline flake composites for high performance supercapacitors, Electrochimica Acta 76 (2012) 62– 68

[62] D. Yuan, T. Zhou, S. Zhou, W. Zou, S. Mo, N. Xia, Nitrogen-enriched carbon nanowires from the direct carbonization of polyaniline nanowires and its electrochemical properties, Electrochemistry Communications 13 (2011) 242–246.

[63] X. Lua, Y. Hua, L. Wanga, Q. Guoa, S. Chena, S. Chena, H. Houa, Y. Songa, Macroporous carbon-nitrogen-dope carbon nanotubes-polyaniline nanocomposites and their application in supercapacitors, Electrochimica Acta 189 (2016) 158–165.

[64] Z. Li, H. Zhang, Q. Liu, L. Sun, L. Stanciu, J. Xie, Fabrication of high-surface-area graphene-polyaniline nanocomposites and their application in supercapacitors, ACS

Applied Materials & Interfaces 5 (2013) 2685–2691.

[65] H. Liu, B. Xu, M. Jia, M. Zhang, B. Cao, X. Zhao, Y. Wang, Polyaniline nanofiber/large mesoporous carbon composites as electrode materials for supercapacitors, Applied Surface Science 332 (2015) 40–46.

[66] W. Wang, Q. Hao, W. Lei, X. Xia, X. Wang, Ternary nitrogen-doped graphene-nickel ferrite-polyaniline nanocomposites for high-performance supercapacitors, Journal of Power Sources 269 (2014) 250-259.

[67] J. Li, M. Cui, Y. Lai, Z. Zhang, H. Lu, J. Fang, Y. Liu, Investigation of polyaniline co-doped with Zn^{2+} and H^{+} as the electrode material for electrochemical supercapacitors, Synthetic Metals 160 (2010) 1228–1233.

[68] P. Xiong, H. Huang, X. Wang, Design and synthesis of ternary cobalt ferrite-graphene-polyaniline hierarchical nanocomposites for high-performance supercapacitors, Journal of Power Sources 245 (2014) 937-946.

[69] K. Kim, S. Park, Influence of multi-walled carbon nanotubes on the electrochemical performance of graphene nanocomposites for supercapacitor electrodes, Electrochimica Acta 56 (2011) 1629–1635.

[70] D. Zhao, X. Guo, Y. Gao, F. Gao, An electrochemical capacitor electrode based on porous carbon spheres hybrided with polyaniline and nanoscale ruthenium oxide, ACS Appl. Mater. Interfaces 4 (2012) 5583–5589.

Figure captions

Fig. 1. Illustration of the experimental procedure for the synthesis of CGP nanocomposites by *in-situ* polymerization.

Fig. 2. Illustration of FT-IR spectra of CS, PANI, CP_5, CG_3P and RGO.

Fig. 3. XRD pattern of CS, PANI, CP_5, RGO and CG_3P.

Fig. 4. Thermograms of CS, PANI, RGO and composites of CP_5 and CG_3P.

Fig. 5. SEM images of PANI (a,b), CP_5 (c,d), RGO (e,f) and CG_3P (g,h) with different magnifications.

Fig. 6. Cyclic voltammograms of PANI, CP_5 and CG_3P measured in three electrode system with a potential range of -1 V to +1 V in 1 M H_2SO_4 electrolyte solution at different scan rates of 5-120 mV s^{-1} (a-c); Cyclic voltammograms of PANI, CP_5 and CG_3P measured at a fixed scan rate of 5 mV s^{-1} (d).

Fig. 7. Variation of the specific capacitance of PANI, CP_5 and CG_3P at different scan rates of 5-120 mV s^{-1} (a); Nyquist plots of PANI, CP_5 and CG_3P (b); Variation of the specific capacitance at different concentration of PANI (c), mass% of RGO (d).

Fig. 8. Galvanostatic charge-discharge curves of the CG_3P, CP_5 and PANI composite electrodes.

Fig. 9. Cycle life stability of PANI, CP_5 and CG_3P at fixed scan rate of 50 mV s^{-1}.

Table 1. Electrical conductivity of samples CP_1 to CP_7, CG_1P to CG_5P, pure PANI and RGO.

Table 2. Comparison of specific capacitance of the developed composite electrode materials with the reported PANI based composite materials.

Figures

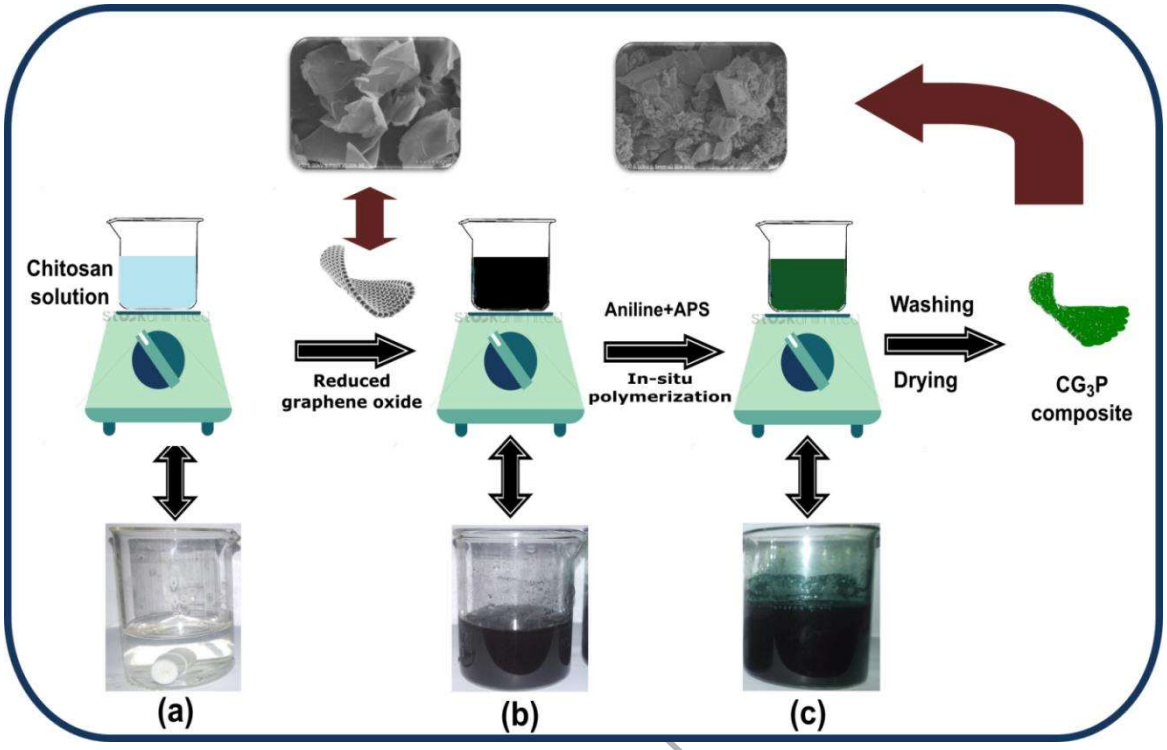

Fig. 1. Illustration of the experimental procedure for the synthesis of CGP nanocomposites by *in-situ* polymerization.

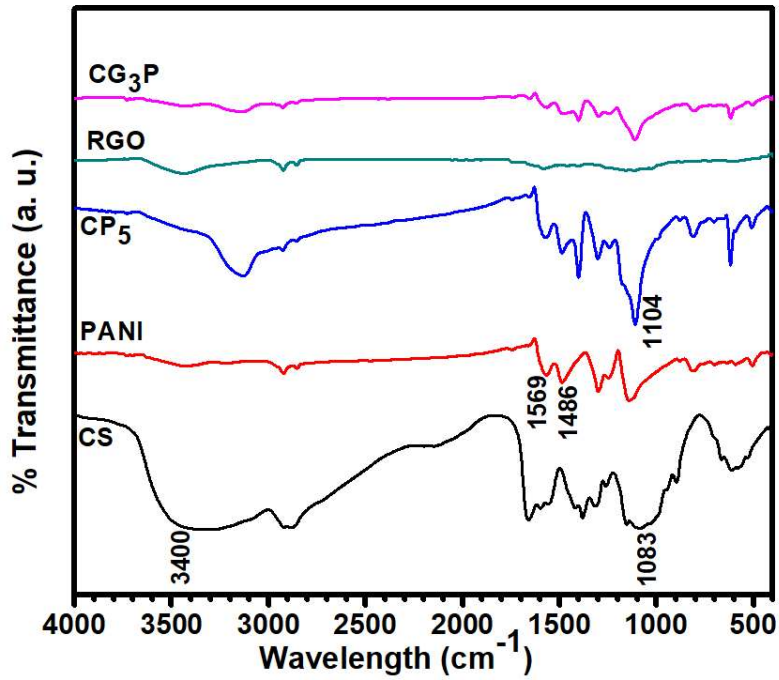

Fig. 2. Illustration of FT-IR spectra of CS, PANI, CP_5, CG_3P and RGO.

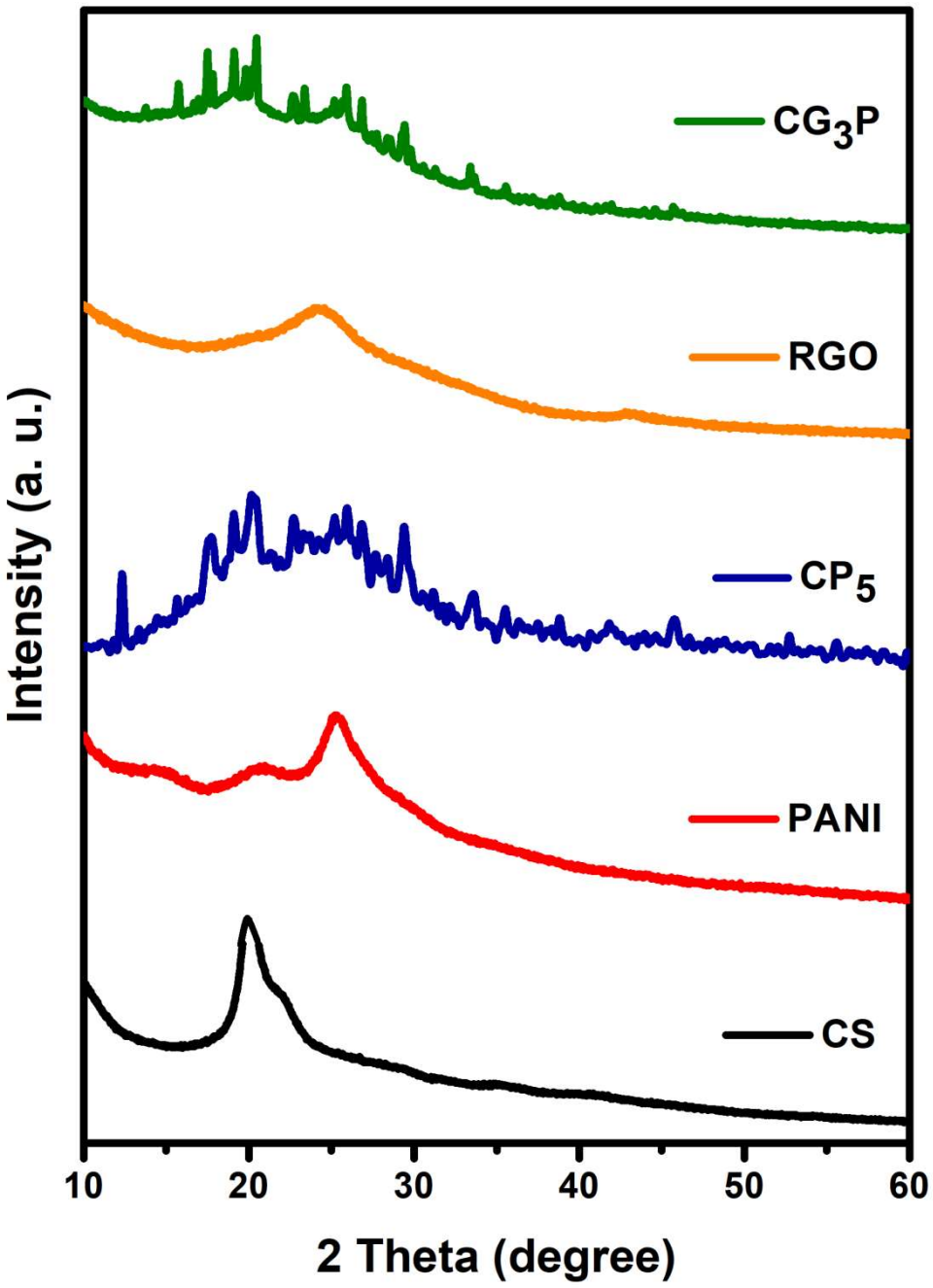

Fig. 3. XRD pattern of CS, PANI, $CP_{5,}$ RGO and CG_3P.

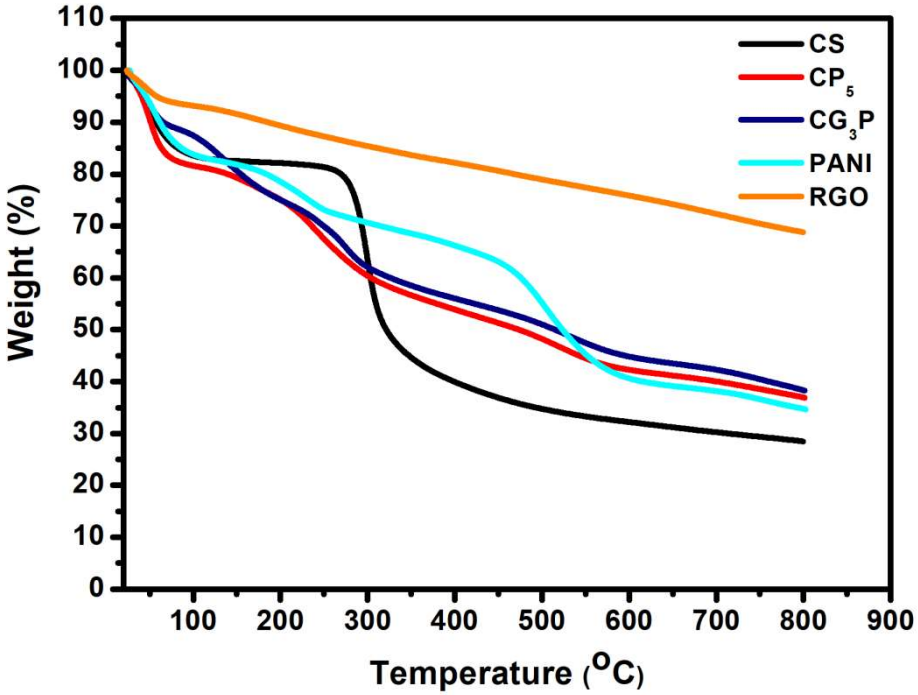

Fig. 4. Thermograms of CS, PANI, RGO and composites of CP_5 and CG_3P.

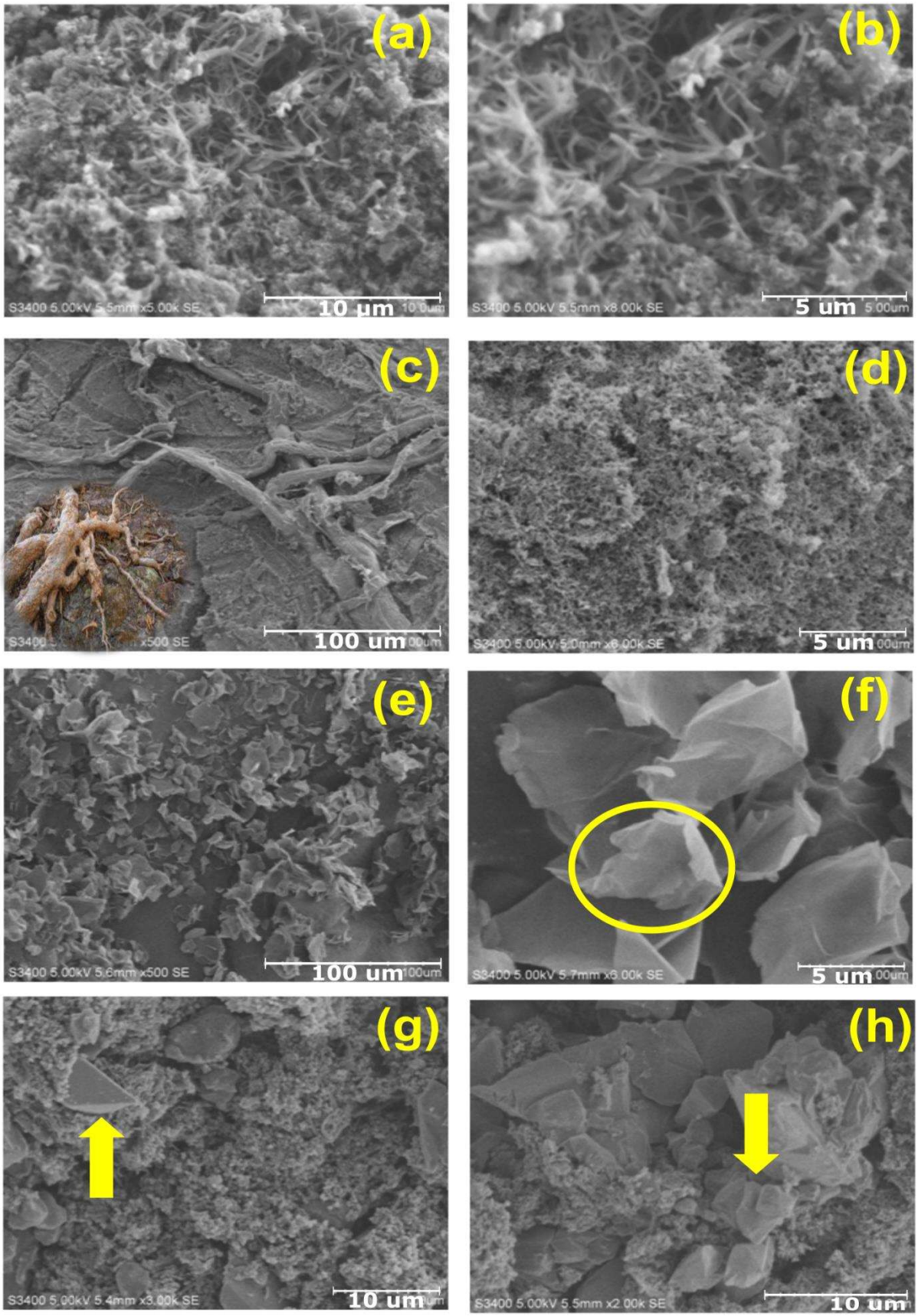

Fig. 5. SEM images of PANI (a,b), CP_5 (c,d), RGO (e,f) and CG_3P (g,h) with different magnifications.

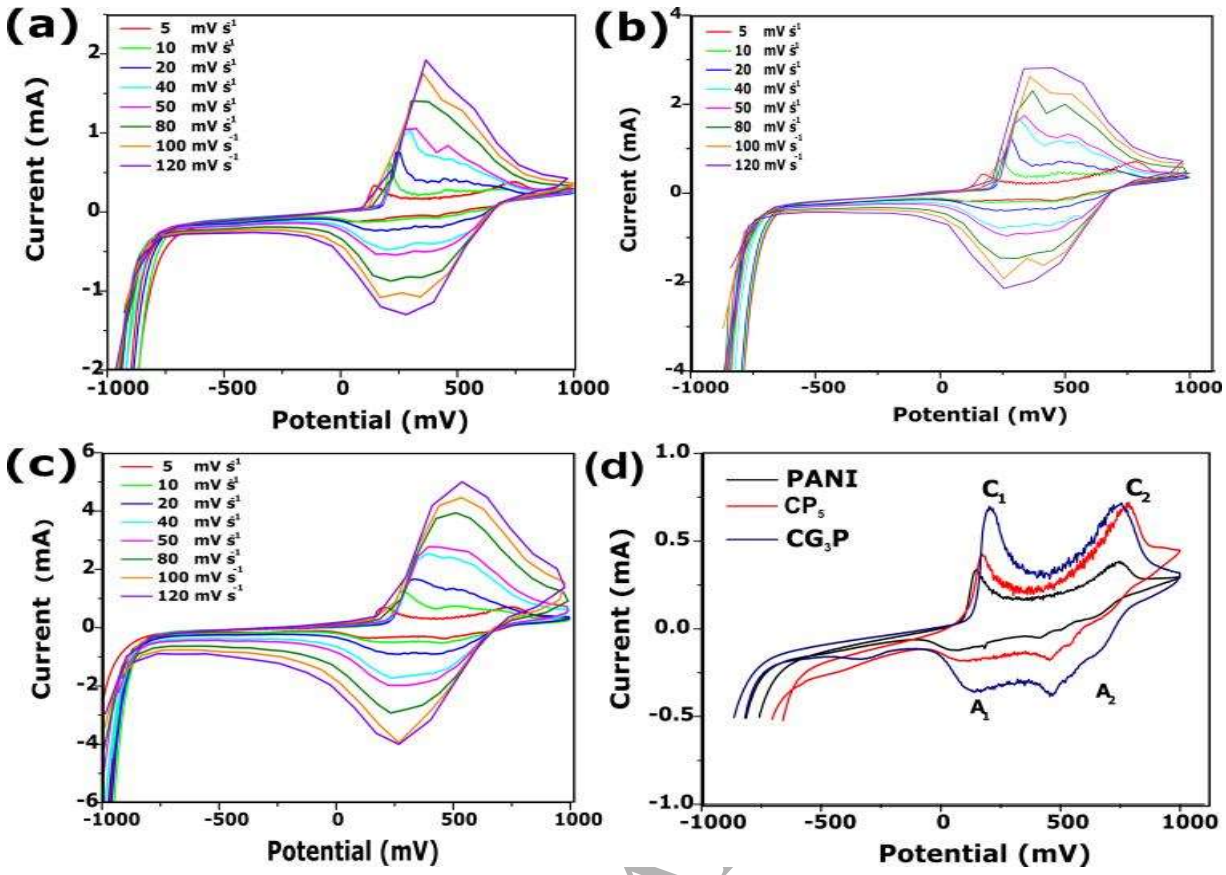

Fig. 6. Cyclic voltammograms of (a) PANI, (b) CP_5 and (c) CG_3P measured in three electrode system with a potential range of -1 V to +1 V in 1 M H_2SO_4 electrolyte solution at different scan rates of 5-120 mV s^{-1}; Cyclic voltammograms of PANI, CP_5 and CG_3P measured at a fixed scan rate of 5 mV s^{-1} (d).

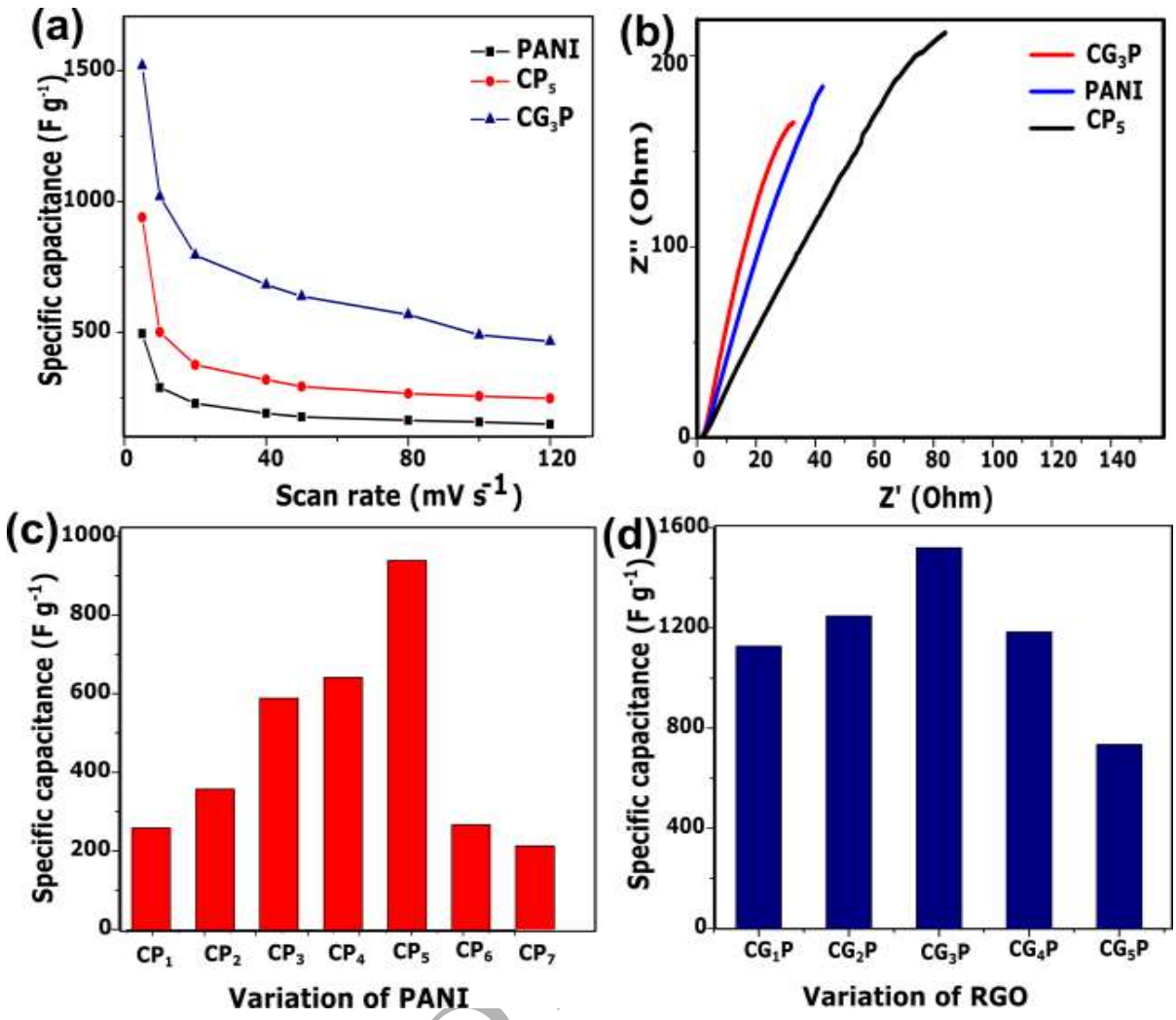

Fig. 7. Variation of the specific capacitance of PANI, CP_5 and CG_3P at different scan rates of 5-120 mV s^{-1} (a); Nyquist plots of PANI, CP_5 and CG_3P (b); Variation of the specific capacitance at different concentration of PANI (c), mass% of RGO (d).

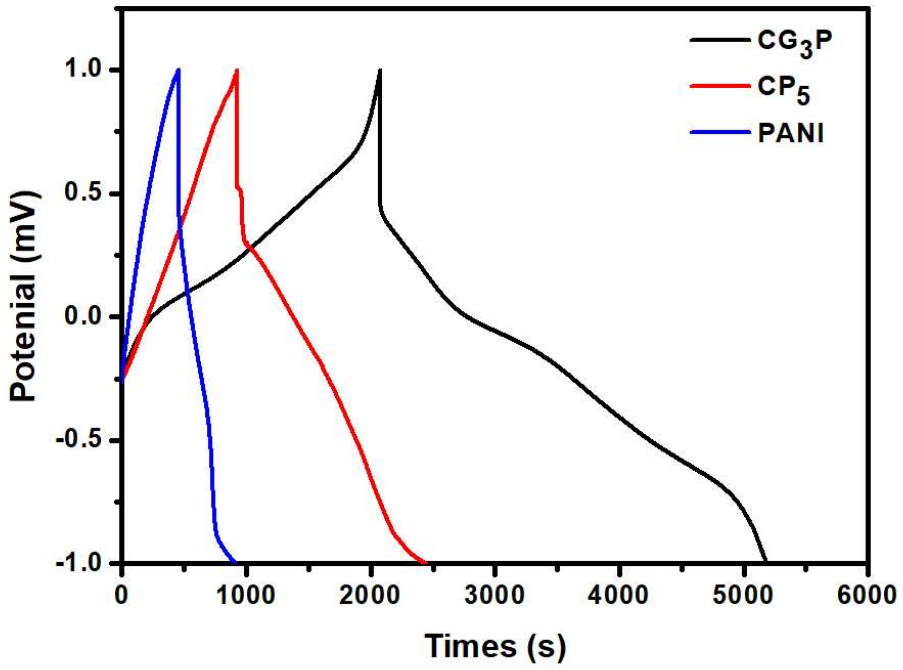

Fig. 8. Galvanostatic charge-discharge curves of the CG_3P, CP_5 and PANI composite electrodes.

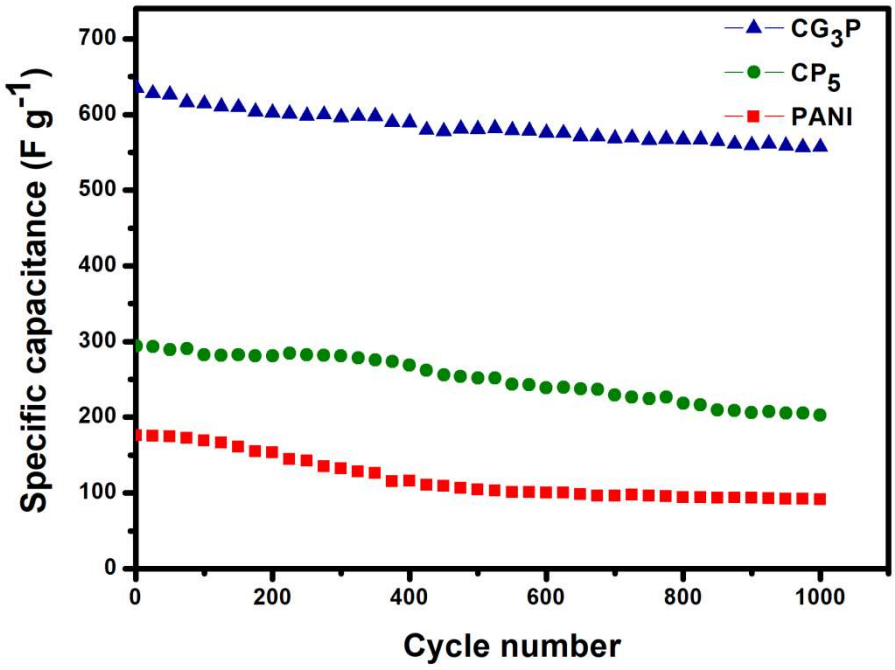

Fig. 9. Cycling life stability of PANI, CP_5 and CG_3P at fixed scan rate of 50 mV s^{-1}.

Table 1 Electrical conductivity of samples CP_1 to CP_7, CG_1P to CG_5P, pure PANI and RGO.

Sample	Electrical conductivity (S cm^{-1})	Sample	Electrical conductivity (S cm^{-1})
CP_1	3.455×10^{-4}	CG_1P	6.343×10^{-1}
CP_2	6.241×10^{-3}	CG_2P	1.10388
CP_3	8.096×10^{-3}	CG_3P	2.9745
CP_4	2.214×10^{-1}	CG_4P	8.125×10^{-2}
CP_5	4.165×10^{-1}	CG_5P	2.002×10^{-2}
CP_6	1.379×10^{-3}	RGO	2.094
CP_7	1.271×10^{-3}	PANI	1.7342

Table 2 Comparison of specific capacitance of the developed composite electrode materials with the reported PANI based composite materials.

Materials	Electrolyte	System	Specific capacitance (F g^{-1})	Reference
CG_3P	1 M H_2SO_4	Three-electrode	1326.82	Present work
PANI	1 M H_2SO_4	Three-electrode	295.48	Present work
GN/PANI/CNT	1 M HCl	Three-electrode	569	60
R(GO/PANI)-3	0.2 M HCl	Three-electrode	764	61
NE-CNWs-700	6 M KOH	Three-electrode	327	62
KSC/NCNT/PANI	2 M H_2SO_4	Three-electrode	1090	63
Graphene/PANI	1 M H_2SO_4	Three-electrode	257	64
PANI-F/LMC	6 M KOH	Three-electrode	473	65
PANI-F	6 M KOH	Three-electrode	21	65
NGNP	1 M KOH	Two-electrode	667	66
PANI co-doped Zn^{2+} and H^+	1.0 M H_2SO_4	Three-electrode	369	67
Polyaniline/Cobalt ferrite/graphene	1 M KOH	Three-electrode	768	68
PANI	1 M KOH	Two-electrode	24.6	68
M-GR/PANI	1.0 M H_2SO_4	Three-electrode	1118	69

GN/PANI/CNT-graphene/polyaniline/carbon nanotubes; GO/PANI-graphene oxide/polyaniline; NE-CNWs-nitrogen-enriched carbon nanowires; KSC/NCNTs/PANI-kenaf stem-derived porous carbon/nitrogen-doped carbon nanotubes/polyaniline; PANI-F/LMC-polyaniline nanofiber/large mesoporous carbon; NGNP-nitrogen-doped graphene/nickel ferrite/polyaniline; M-GR-multi-walled carbon nanotube (MWNT) bonded graphene.

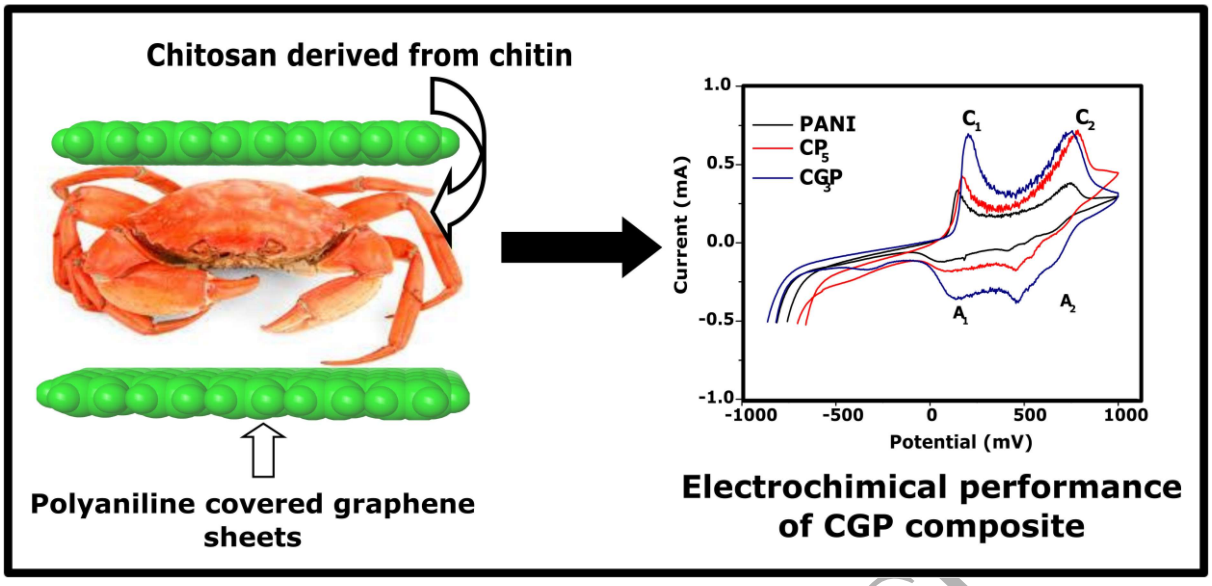

Graphical abstract